Materials Horizons

# Tailoring the thermal conductivity of two-dimensional metal halide perovskites



| | |
|---|---|
| Journal: | *Materials Horizons* |
| Manuscript ID | MH-COM-08-2022-001070.R1 |
| Article Type: | Communication |
| Date Submitted by the Author: | 03-Oct-2022 |
| Complete List of Authors: | Thakur, Sandip; University of Rhode Island<br>Dai, Zhenghong; Brown University, School of Engineering<br>Karna, Pravin; University of Rhode Island<br>Padture, Nitin; Brown University, School of Engineering<br>Giri, Ashutosh; University of Virginia, |
| | |

Arising from their unrivalled optoelectronic properties, two-dimensional (2D) metal halide perovskites (MHPs) have paved new paths forward as tailor-made semiconductors for solar cell applications. Their enhanced thermal stability as compared to their three-dimensional counterparts positions them as the next generation materials to revolutionize energy storage and conversion. However, still one of the biggest challenges for their large scale incorporation in photovoltaic devices is the issue of their proper thermal management, which arises from their inherently ultralow thermal conductivities and the limited understanding of the heat transfer processes in these novel materials. Herein, we provide a detailed analysis of the thermal transport mechanisms in 2D MHPs through both experimental and computational approaches demonstrating a novel strategy to engineer enhanced thermal conductivities in these materials. In contrast to conventional approaches utilized to increase thermal conductivity in layered materials (such as by decreasing interfacial scattering of phonons via reducing the interface density), we show that decreasing the distance between adjacent organic cations can lead to more than four-fold increase in thermal conductivity, thus facilitating the potential use of these materials for wide-spread applications in solar cells with enhanced efficiencies.

Journal Name

ARTICLE TYPE

Cite this: DOI: 00.0000/xxxxxxxxxx

# Tailoring the Thermal Conductivity of Two-Dimensional Metal Halide Perovskites†

Sandip Thakur,‡[a] Zhenghong Dai,‡[b] Pravin Karna,[a] Nitin P. Padture,[b] and Ashutosh Giri*[a]

Received Date
Accepted Date

DOI: 00.0000/xxxxxxxxxx

Proper thermal management of solar cells based on metal halide perovskites (MHPs) is key to increasing their efficiency as well as their durability. Although two-dimensional (2D) MHPs possess enhanced thermal stability as compared to their three-dimensional (3D) counterparts, the lack of comprehensive knowledge of the heat transfer mechanisms dictating their ultralow thermal conductivities is a bottleneck for further improvements in their thermal performance. Here, we experimentally and computationally study the Dion-Jacobson (DJ) and Ruddlesden-Popper (RP) phases of MHPs (n=1) to demonstrate that the length of the organic spacers has a negligible influence on their thermal transport properties; we experimentally measure thermal conductivities of 0.19±0.03 W m$^{-1}$ K$^{-1}$ and 0.18±0.03 W m$^{-1}$ K$^{-1}$ for the RP and DJ phases with 13.6 Å and 6.3 Å interlayer inorganic separations, respectively. In contrast, we show that thermal conductivity is mainly dependent on the separation between the adjacent organic cations. Decreasing the intermolecular distance (by up to 40%) leads to drastically enhanced overall heat conduction (with monotonically increasing thermal conductivity by more than threefold) which is mainly driven by the vibrational hardening of the organic spacers. Although these 2D layered materials constitute a high density of hybrid organic-inorganic interfaces, our results also show that a substantial portion of heat is conducted through coherent phonon transport and that the thermal conductivity of these materials is not solely limited by incoherent interfacial scattering.

Metal halide perovskites (MHPs) such as methylammonium lead iodide ($MAPbI_3$) have emerged as game-changing materials for a plethora of applications in the next generation of photovoltaics, light-emitting diodes, photodetectors, optoelectronics, and thermoelectrics due to their remarkable physical properties.[1–6] Most notably, their enhanced carrier lifetimes,[7–10] facile processability,[11–15] and high absorption coefficients[16] have been exploited to increase their power conversion efficiencies to greater than 25% in $MAPbI_3$-based solar cells.[17] However, one of the major bottlenecks for their large-scale incorporation in devices (such as in solar cell applications) is the issue of their instability, where these materials rapidly degrade under exposure to moisture, oxygen, light, or elevated temperatures.[18] In this regard, the two-dimensional (2D) versions of MHPs such as the Ruddlesden-Popper (RP) phases have recently garnered much attention due to their enhanced stability as compared to their 3D counterparts.[19,20] These layered MHPs exhibit many of the superior optoelectronic properties of their 3D cousins, all the while demonstrating some of the exceptional qualities that accompany 2D semiconductors, such as possessing quantum confinement characteristics.[21] Although 2D MHPs mark a drastic improvement in terms of thermal stability, their exceptionally low thermal conductivities (reported to be in the 0.12-0.37 W m$^{-1}$ K$^{-1}$ range for 2D alkylammonium lead iodide,[22–25] for example) makes their proper thermal management and the complete understanding of their heat transfer mechanisms quintessential for further improvements in their thermal stability and their usage in current technology.

Recently, a number of reports have focused on describing thermal transport in 2D MHPs. Christodoulides *et al.*,[23] measured the through-plane thermal conductivity of $MAPbI_3$-based RP phase perovskites to be 0.37±0.13 W m$^{-1}$ K$^{-1}$, a value comparable to their 3D counterparts.[26,27] However, increasing the number of inorganic layers (n) separated by organic spacers was shown to drastically reduce the thermal conductivity (to ∼0.06±0.03 W m$^{-1}$ K$^{-1}$), which they attributed to a reduction in coherent phonon transport that limits heat transfer in the RP phase perovskites with thicker inorganic layers. Considering the high density of inorganic-organic interfaces, along with the reduced sound speeds and elastic constants in the through-plane

[a] *Department of Mechanical, Industrial and Systems Engineering, University of Rhode Island, Kingston, RI 02881, USA. E-mail: ashgiri@uri.edu*
[b] *School of Engineering, Brown University, Providence, Rhode Island 02912, USA*

† Electronic Supplementary Information (ESI) available: Sample preparation and characterization; details on TDTR measurements and analysis; details on MD simulations, NEMD simulations, volumetric heat capacity, vibrational density of states, and electronic band gap calculation. See DOI: 00.0000/00000000.

‡ These authors contributed equally to this work.

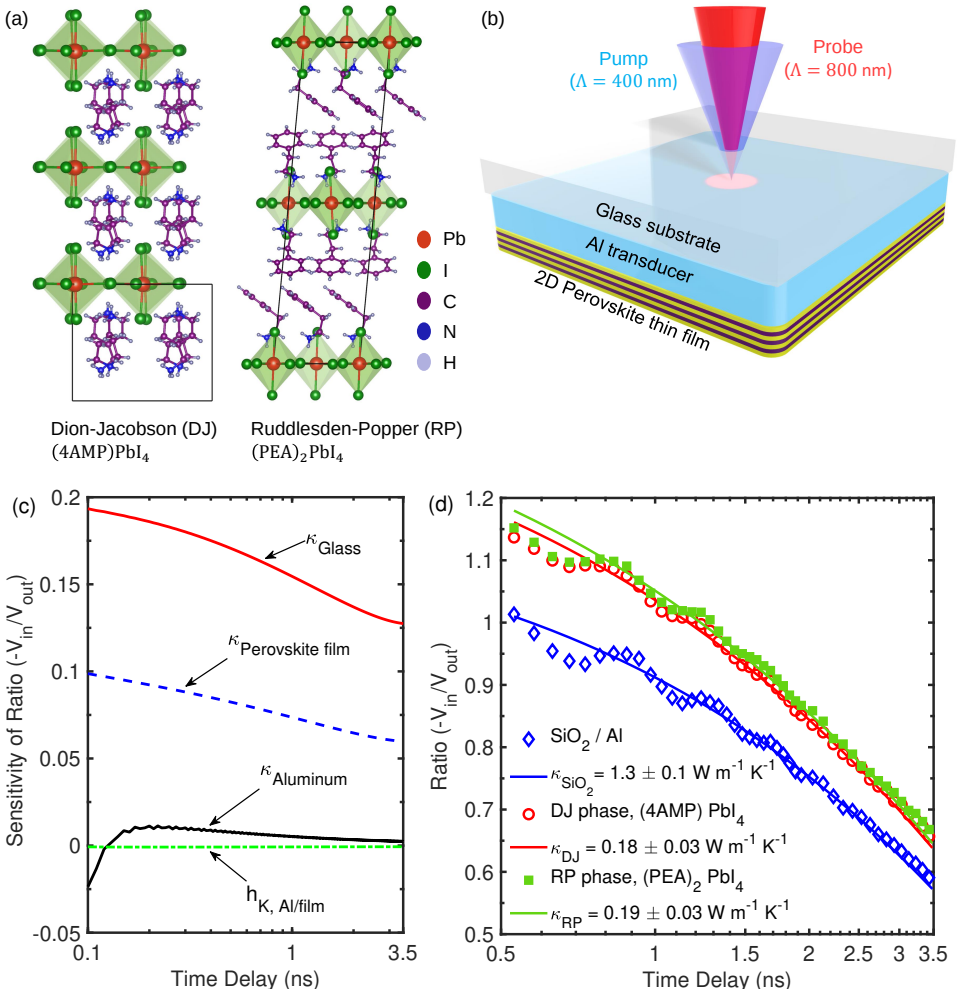


**Fig. 1** (a) Crystal structure of the DJ phase $\left((4AMP)PbI_4\right)$ and RP phase $\left((PEA)_2PbI_4\right)$ MHPs showing the unit cells. The unit cell for the DJ phase is substantially smaller as compared to the RP phase due to the pairs of interdigitated interlayer organic spacers in the RP phase. (b) Schematic of our thermal measurements via TDTR experiments on our three layered system (glass/Al/hybrid perovskite film). A pump laser (blue) heats the Al transducer layer while a probe (red) beam measures the temperature changes on the surface of the transducer as a function of pump-probe time delay to accurately measure the thermal conductivity of the 2D perovskite film. (c) Sensitivities of the ratio of the in-phase ($V_{\rm in}$) and out-of-phase ($V_{\rm out}$) signals to the parameters used in the thermal model as a function of delay time. (d) Representative TDTR data for the $(PEA)_2PbI_4$ (green squares) and $(4AMP)PbI_4$ (red circles) thin films and their corresponding best fit thermal models. The TDTR data of our calibration sample (without the perovskite thin film) is also shown for comparison, which is used to accurately determine the thermal conductivity of the glass substrate used as an input parameter in our three-layer thermal model.

direction (perpendicular to the layers), it might be expected that the thermal conductivity of the 2D MHPs would be lower in comparison to their 3D counterparts. However, crystal imperfections such as grain boundaries and defects in 3D $MAPbI_3$ that scatter phonons and lower the thermal conductivity could be one of the causes for the similarity in the thermal conductivities between the single crystal 2D RP phase measured by Christodoulides *et al.*[23] and the 3D counterparts.[26,27] In contrast, three other reports have independently measured lower values of thermal conductivity in the 0.13-0.2 W $m^{-1}$ $K^{-1}$ range for the $MAPbI_3$-based RP phase perovskites.[22,24,25] The discrepancies between the measurements in the various aforementioned works may have arisen due to variations in film preparation procedures and conditions such as the use of different solvents and substrate temperatures during deposition that have been shown to impact film morphologies.[28–31]

Rasel *et al.*[25] experimentally demonstrated that varying the chain length of the alkylammonium cations from 13.8 to 18.03 Å range did not significantly alter the thermal conductivity of 2D MHPs. Similarly, Giri *et al.*[22] measured the thermal conductivities of eight different 2D MHPs with varying organic cations (that have chain lengths in the 13.07 to 16.67 Å range) and found that the thermal conductivity did not depend on the organic cation species, but rather depended on the orientation and arrangement of the organic spacers in the films. These results suggest that the thermal conductivities in these RP phase perovskites are not limited by incoherent scattering of vibrations at the hybrid inorganic-organic interface because one would expect a linearly increasing thermal conductivity with increasing chain length. Therefore, the lack of chain length de-

pendence could in part be due to coherent phonon transport (inline with the findings of Christodoulides *et al.*[23]). It could also arise, however, from the fact that the change in thermal conductivity by varying the length of the organic spacers by ∼4 Å (and considering the fact that the organic cations in the RP phase are comprised of pairs of interdigitated interlayer organic spacers) in these works, might not be discernible within the experimental uncertainties. In other words, along with vibrational scattering at the hybrid interfaces (estimated to reduce the thermal conductivity by ∼30% when the organic chain length is increased from 13.8 to 18.03 Å),[25] the thermal conductivity in these materials could also likely be limited by scattering at the organic-organic interfaces; in the RP phases, the organic cations only interact with the negatively charged halides in the inorganic layers at one end of their chain forming a weak van der Waals gap between the organic cations in the adjacent layers (see Fig. 1a). Thus, if it is expected that considerable vibrational scattering occurs at these weak van der Waals interfaces, a small increase in the length of the organic spacers might not translate to an observable change in thermal conductivity within the typical uncertainties in time-domain thermoreflectance (TDTR) experiments. Taken together, although the aforementioned studies suggest that there are signatures of coherent phonon transport in the through-plane direction of the various RP phase perovskites, the intrinsic mechanism of heat transfer in 2D MHPs is still unclear with several questions, such as the role of the weak van der Waals gap between the adjacent organic cations in influencing their overall thermal conductivities, left unanswered.

Herein, we experimentally and computationally study the heat transfer mechanisms across 2D MHPs (n=1) to elucidate the role of the weak van der Waals gap between the adjacent organic layers and to rationalize a strategy to efficiently tailor their thermal properties across a wide range. We do so by conducting TDTR experiments and performing molecular dynamics (MD) simulations on the Dion-Jacobson (DJ) phase ((4AMP)$PbI_4$; AMP = aminomethyl piperidinium) and RP phase ($(PEA)_2PbI_4$; PEA = phenylethyl ammonium) MHPs. The comparison between the RP phase and the DJ phase (without the van der Waals gap as illustrated in Fig. 1a), allows us to examine the role of the weak organic-organic interactions in dictating their thermal conductivity. It also allows us to compare the effect of the much shorter organic spacers in between the 2D inorganic layers (which is ∼6.3 Å for the DJ phase as opposed to the ∼13.1 to 16.8 Å organic spacer lengths studied in prior works for the RP phases) on the heat transfer mechanisms in these MHPs. Our results from the TDTR experiments and MD simulations unequivocally show that both the length of the organic spacer and the van der Waals gap between the organic cations have negligible effect on the thermal conductivity of these 2D perovskites as demonstrated by the similarity in the thermal conductivities of the DJ and RP phases. Our atomistic simulations reveal that coherent phonons can carry an appreciable portion of heat across the interfaces without scattering at the high density of interfaces. However, our results also suggest that scattering due to disorder and imperfections (such as scattering at the hybrid interfaces) in these MHPs can also influence their thermal conductivity. We show that rather than changing the organic spacer length, decreasing the distance between the adjacent organic cations can result in drastic enhancements in their thermal conductivity. We attribute this to vibrational hardening of the organic species due to reduction in the lateral spacing between the organic chains that drives the increase in both the in-plane and through-plane thermal conductivities.

We study the thermal properties of DJ phase (4AMP)$PbI_4$ and RP phase $(PEA)_2PbI_4$ thin films with ∼600 nm thickness that are deposited on top of a 100 nm thick Al film on glass substrate. The details of the sample fabrication and characterization are given in the Supporting Information. Figures S1a and S1b show the X-ray diffraction (XRD) patterns of our RP and DJ phase hybrid perovskite films which highlight their excellent crystallinity and layered structure with respect to the substrate.

We use TDTR to measure the thermal conductivities of our thin films at room temperature. The details of the experimental setup and the analysis procedure are given elsewhere,[32–34] and the specifics of our experiments are given in the Supporting Information. Briefly, TDTR is a non-contact, pump-probe technique that utilizes a modulated short pulse laser (with ∼100 fs pulse width) to create a periodic heating event (pump) on the surface of a transducer layer (that is the 100 nm Al thin film in our experiments). A time-delayed probe pulse monitors the change in reflectivity that is related to the change in temperature of the transducer layer at the modulation frequency of the pump, which is detected by a lock-in amplifier. For our experiments, we focus the pump and probe pulses through the transparent glass substrate on the Al transducer layer as illustrated in the schematic in Fig. 1b.

A three-layer thermal model is used to predict the temperature change on the surface of the Al transducer, which is related to the thermal conductivity, heat capacity of the composite slabs and the thermal boundary conductance across each interface between the slabs. Figure 1c shows the sensitivities of the various thermophysical parameters in our thermal model to our TDTR data. In our experimental configuration, the most sensitive parameter is the thermal conductivity of the glass substrate. Therefore, to accurately determine the thermal conductivity of our hybrid perovskite films, we first measure the thermal conductivity of our glass substrate with a control sample (without the hybrid perovskite film). As shown in Fig. 1d, we accurately measure the thermal conductivity of the glass substrate (which agrees well with prior literature value)[35] by fitting a two-layer thermal model shown as the solid line to our TDTR data taken on the control sample. We use this as an input parameter in the three-layer thermal model to measure the thermal conductivities of our DJ phase and RP phase thin films as shown in Fig. 1d. For both phases, we measure a thermal conductivity of ∼0.19 W $m^{-1}$ $K^{-1}$ much lower than the 0.34 to 0.73 W $m^{-1}$ $K^{-1}$measured for their 3D counterparts using a similar pump-probe metrology.[27]

The similarity in the measured thermal conductivities for the two different phases is surprising since the RP phase is comprised of pairs of interdigitated interlayer organic spacers, while the DJ phase only has one cation per formula unit, which leads to a reduced separation between the inorganic layers in the DJ phase (see Fig. 1a).[22,36] If the hybrid interfaces are expected to limit

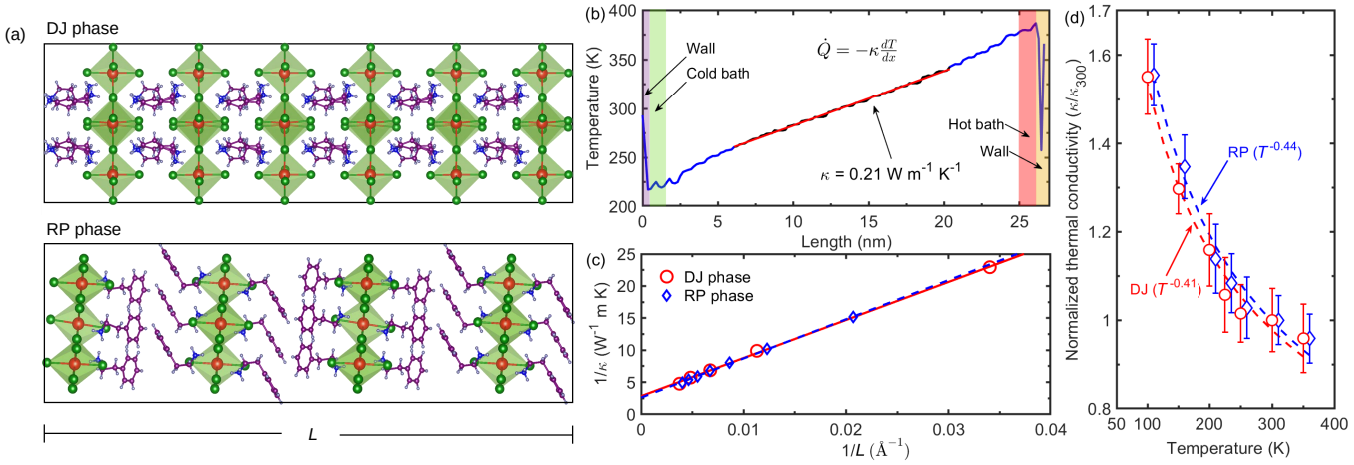


**Fig. 2** (a) Schematics of our computational domains for the DJ and RP phases showing the relatively higher hybrid interface densities in the DJ phase compared to the RP phase. (b) An example of the temperature gradient profile for a computational domain of the DJ phase obtained with the NEMD approach where a heat flux is applied in the through-plane direction. By invoking the Fourier's law, we can determine the thermal conductivity in the direction of the applied heat flux. (c) To predict the 'bulk' thermal conductivities of the RP and DJ phases, we plot the inverse of $\kappa$ as a function of the inverse of the computational domain length ($L$) in the direction of heat flux applied. The extrapolation of the linear fits to $1/L \rightarrow 0$ predicts the thermal conductivity of the 'bulk' system. (d) NEMD-predicted thermal conductivities of our DJ and RP phases (normalized by the thermal conductivity of the DJ phase at 300 K) in the through-plane direction as a function of temperature. The thermal conductivity follows a crystalline-like temperature dependence where the thermal conductivity decreases with temperature, which is mainly attributed to anharmonic phonon-phonon scattering. This shows that for both phases, substantial amount of heat is carried by coherent phonon transport across the inorganic and organic layers.

phonon transport through incoherent scattering, one would expect the DJ phase with the higher density of interfaces to possess lower thermal conductivity in comparison to the RP phase. The similarity in the measured thermal conductivity, however, suggests that interfacial scattering may not be the dominant mechanism dictating heat transfer in these materials. Along with the hybrid interfaces, if the non-bonded interactions between the pair of organic spacers in the RP phase is also expected to scatter the phonons via interfacial scattering at the weak organic-organic interfaces, the similarity in the measured thermal conductivities could arise due to comparable interface densities in the two phases. Therefore, to unravel these various scattering mechanisms that dictate thermal conductivity in 2D MHPs, we perform MD simulations on the two phases by utilizing the MYP potential for hybrid perovskites that has been shown to replicate the structural and elastic properties,[37] as well as the ionic polarizations[38,39] and mobilities[40] in these materials (further details of the simulations are given in the Supporting Information).[41]

Figure 2a shows example schematics of our MD computational domains, where the dissimilarity in the length of the organic spacers lead to interlayer distances of ~6.3 Å and ~13.6 Å for the DJ and RP phases, respectively. These separations for our relaxed structures are within 10% of the experimentally determined lengths, which further validates our use of the MYP potential to describe the thermal properties of these hybrid perovskites. To calculate their thermal conductivities, we perform nonequilibrium MD (NEMD) simulations where we prescribe hot and cold baths at opposite ends of the simulation domain to create steady-state temperature profiles from which we predict the thermal conductivity by invoking the Fourier's law as shown in Fig. 2b for our DJ phase computational domain. If longer wavelength phonons scatter at and near the heat baths, the NEMD-predicted thermal conductivities will be limited by the computational domain length ($L$) in the direction of the applied heat flux.[42] As shown in Fig. 2c, we plot the inverse of thermal conductivity ($1/\kappa$) versus $1/L$ to extract the 'bulk' thermal conductivity (by extrapolating to $1/L$=0). We observe a monotonic increase in the thermal conductivity for both phases with increasing domain length suggesting that coherent phonons can carry a significant portion of heat in these hybrid materials. Moreover, similar to our experimental results, we calculate similar values of 'bulk' thermal conductivities for the two phases. However, our NEMD simulations predict a thermal conductivity of ~0.38 W m$^{-1}$ K$^{-1}$, which is higher than our TDTR measurements but agrees very well with Christodoulides *et al.*'s[23] measurement on single crystals of the RP phase hybrid perovskite. The discrepancies between our NEMD results and TDTR experiments could be due to the crystalline imperfections such as grain boundaries that result in additional phonon scattering leading to the lower thermal conductivities measured by TDTR for these materials. We note that our additional NEMD calculations on 3D $MAPbI_3$ (which are in-line with prior MD simulation results as detailed in the Supporting Information) are also higher as compared to experimental measurements,[27] which is also most likely due to structural imperfections (defects, dislocations, etc.) lowering the measured thermal conductivities in the experiments.

To further understand the phonon scattering mechanisms dictating thermal transport in these hybrid perovskites, we calculate the temperature-dependent thermal conductivities via NEMD simulations as shown in Fig. 2d. For both phases, the thermal conductivities show a crystalline-like behavior where the thermal conductivity increases with decreasing temperature. This is indicative of anharmonic phonon-phonon scattering mechanisms dictating the temperature dependence, albeit with a weaker de-

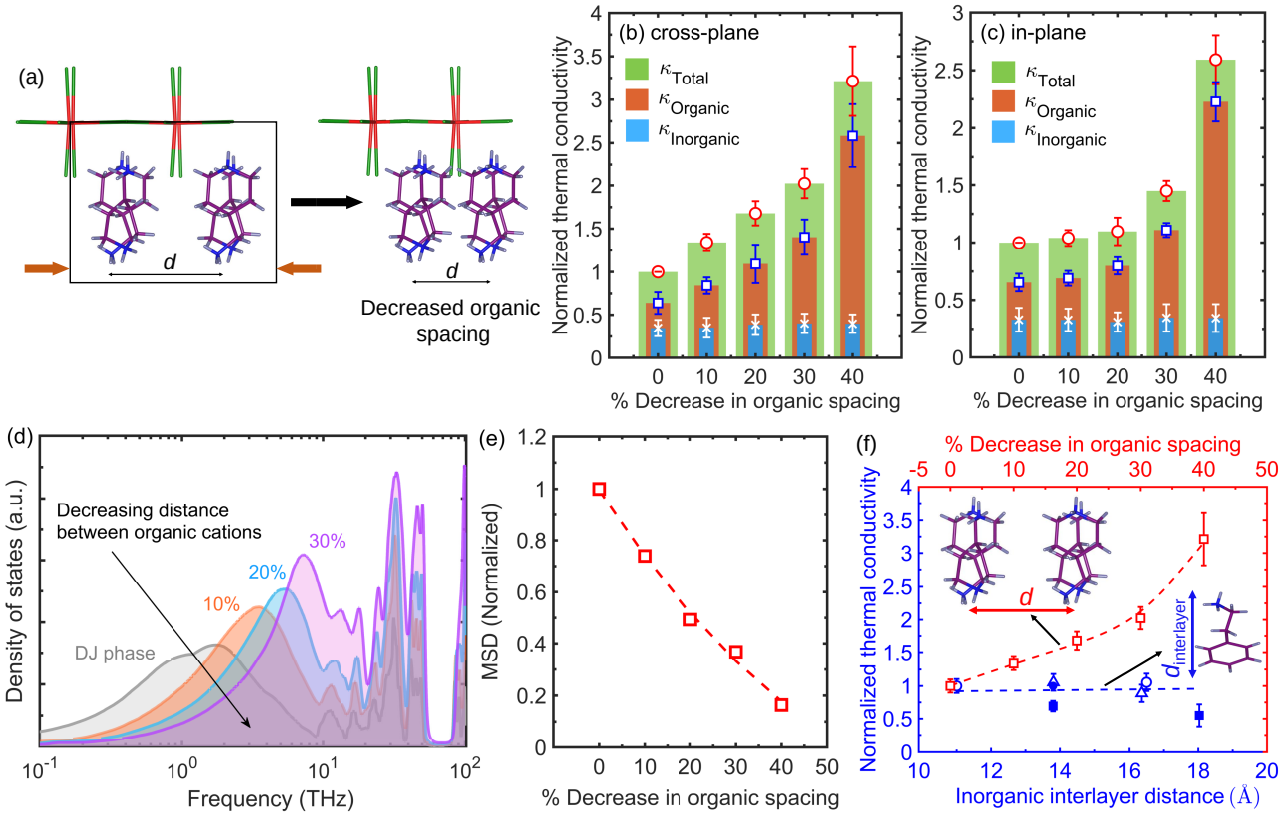


**Fig. 3** (a) Schematic illustration showing the variation in organic spacing ($d$) that we simulate in our MD calculations. Normalized thermal conductivities (with respect to the DJ phase) in the (b) through-plane (c) in-plane directions as a function of percentage decrease in $d$ for our DJ phase. In both directions, decreasing $d$ leads to enhanced heat transfer mainly driven by the organic cations. (d) Vibrational density of states for the structures with decreasing $d$ as compared to that of the realistic DJ phase. Considerable vibrational hardening is observed with decreasing spacing between the organic cations. (e) Calculated mean square displacements of the organic cations as a function of decreasing distance between the organic cations. (f) Normalized through-plane thermal conductivities (with respect to the DJ phase) as a function of increasing inorganic interlayer distances (blue; bottom axis) and decreasing distance between organic layers (red; top axis). The red hollow square symbols are results from our NEMD simulations while the blue hollow circle symbols are our TDTR measurements. The other symbols represent experimental measurements taken from Ref. 22 (hollow triangles), Ref. 24 (solid circle), and Ref. 25 (solid square). Changing the inorganic layer separation has negligible effect, while decreasing the separation between adjacent organic cations can drastically increase the thermal conductivity of 2D MHPs.

pendence as compared to pure crystalline solids (i.e. $\kappa \sim T^{-1}$ driven by Umklapp scattering processes). The weaker dependence indicates that along with anharmonic phonon-phonon scattering, additional scattering through 'disorder' (such as interface scattering and scattering due to heterogeneities in the force constants between the various atoms) is also driving the temperature-dependent thermal conductivities in these materials. Taken together, our NEMD results unequivocally show that along with incoherent scattering, significant amount of heat is also transported by phonons that are coherent across the unit cell that scatter due to anharmonic processes.

If we expect the weaker van der Waals interactions between the pair of organic cations in the RP phase to significantly scatter phonons, the cations will have a reduced contribution to the total thermal conductivity when compared to the DJ phase. However, for both phases we calculate ~60% contribution from the organic spacers (see Supporting Information for details) indicating that the van der Waals interactions does not significantly affect the thermal conductivity in these materials. Moreover, we calculate similar thermal conductivities for our RP phase and a DJ phase perovskite with an increased organic spacer length that matches the spacer length in the RP phase (see Fig. S7 in the Supporting Information). Although weaker van der Waals interactions exists in the RP phase perovskite compared to the DJ phase, the similarity in the thermal conductivities even with a longer organic spacer for the DJ phase suggests that the van der Waals interactions has negligible influence in dictating the thermal transport properties in these hybrid perovskites. Furthermore, we summarize prior measurements of thermal conductivity performed on various 2D hybrid MHPs with varying interlayer distance between the inorganic layers (such as $BA_2PbI_4$; BA = butyl ammonium), and compare the results to our measurements on $(4AMP)PbI_4$ and $(PEA)_2PbI_4$ in Table 1. The similarity in the thermal conductivities for inorganic interlayer separation lengths in the range of 10.9-18.03 Å suggests that the organic spacer length has negligible effect on the thermal conductivities of these 2D MHPs. Thus, if the distance between the interlayers do not affect the through-plane thermal conductivity in these materials, the other possibility could be that the distance between the adjacent organic cations limits heat conduction in these hybrid perovskites.

To investigate the validity of this conjecture, we conduct additional simulations on our computational domains where we systematically decrease the distance between the organic spacers as schematically illustrated in Fig. 3a, the results of which we will discuss next. We note that the change in the separation between the organic cations (such as by manipulating the metal-halide bond lengths) in MHPs can result in further structural changes such as octahedral tilting and metal halide bond contractions.[43–45] As such, this might influence other physical properties such as their optical and photophysical characteristics.[46] For example, Jaffe *et al.*[47] have summarized the effect of pressure (and change in lattice constants) on the electronic landscape and excited state dynamics in MHPs. For hybrid perovskites, it has been shown that pressures of $> 50$ GPa are required to change the materials from a semiconducting to a metallic state.[48,49] We note that the pressures induced in our NEMD simulations are less than 23 GPa, and so the thermal transport in these systems are still vibrationally-driven, with negligible contributions from the electronic systems.

**Table 1** Interlayer distance between the inorganic layers ($d$) and room temperature thermal conductivity ($\kappa$) of various 2D MHPs.

| Type | $d$ (Å) | $\kappa$ (W m$^{-1}$ K$^{-1}$) |
|---|---|---|
| (4AMP)$PbI_4$ | 10.9 | $0.18 \pm 0.03$ |
| $(C_4H_9NH_3)_2PbI_4$ | 13.8 | $0.125 \pm 0.01$ (Ref. 25) |
| n$BA_2PbI_4$ | 13.8 | $0.18 \pm 0.04$ (Ref. 22) |
| $BA_2PbI_4$ | 13.8 | $0.18 \pm 0.01$ (Ref. 24) |
| (PEA)$PbI_4$ | 16.36 | $0.15 \pm 0.03$ (Ref. 22) |
| $(PEA)_2PbI_4$ | 16.5 | $0.19 \pm 0.03$ |
| $(C_4H_9NH_3)_2PbI_4$ | 18.03 | $0.099 \pm 0.03$ (Ref. 25) |

Figures 3b and 3c show the normalized thermal conductivity (with respect to the relaxed computational domain) of our DJ phase in the through-plane and in-plane directions, respecitvely, as the distance between the organic cations is decreased. For both the through-plane and in-plane directions, we observe a monotonic increase in thermal conductivity as the separation is decreased. Furthermore, this increase is solely due to the increasing contributions from the organic cations in both directions. The increase in thermal conductivity with decreasing separation between the organic spacers can be ascribed to vibrational hardening where the vibrational spectrum of the organic cations are shifted to higher frequencies as shown in Fig. 3d. Furthermore, the mean square displacements of the atoms comprising the organic spacers also decrease monotonically as the vibrations harden (Fig. 3e), thus leading to an increase in the overall thermal conductivity. These results emphasize the significant role of organic cation separation more-so than the separation between the inorganic layers in dictating the thermal conductivity of these 2D hybrid perovskites. Considering this, a strategy to increase heat conduction in these materials would be to alter the organic-inorganic interactions to dictate the separation between the adjacent organic spacers. We note that the increase in thermal conductivity for the RP phase is even more pronounced than the DJ phase with decreasing separation between adjacent organic cations as the RP phase is comprised of pairs of organic cations as opposed to the single cation in the DJ phase. Therefore, a more pronounced effect is observed on the mean square displacements and the vibrational spectrum of the organic spacers that control the thermal conductivity in the RP phase (see Fig. S9 and Fig. S10 of the Supporting Information), which further solidifies our conjecture.

Experimentally, the distance between the adjacent organic cations can be tuned either by synthetic manipulation, i.e., by manipulating the metal-halide bond lengths by varying the organic cations ($Cs^+$, $MA^+$, or $FA^+$) or inorganic elements ($Pb^{2+}$, $Sn^{2+}$, $Ge^{2+}$, $Cu^{2+}$, $Cd^{2+}$, $Cl^-$, $Br^-$, or $I^-$), or by application of external stimuli (such as pressure),[47,50] which can change the inorganic bond length and polyhedral distortions. This change can vary the separation between the adjacent organic cations to maintain the overall charge neutrality. For example, in prior literature,[51] it has been shown that the lattice parameter of $(MA)_2PbI_2(SCN)_2$ changes by $\sim 8\%$ at $\sim 3.9$ GPa pressure, which can further be decreased with increasing pressure.[47] As such, a detailed experimental investigation on the effect of changing the metal-halide bond length on the thermal conductivity deserves further investigation, but is beyond the scope of the current work.

In summary, we comprehensively show that the interlayer distance between the inorganic layers have minimal effect on the thermal conductivity of 2D hybrid perovskites as shown in Fig. 3f. To tailor their thermal properties, however, a better strategy is to decrease the spacing between the organic cations. We show that decreasing the organic spacing by $\sim$40% can lead to $\sim$200% increase in thermal conductivity of the DJ phase (4AMP)$PbI_4$ (see Fig. 3f). This is attributed to the enhancement in heat conduction that is solely driven by the organic cations, which stiffen due to the increasing interactions from the adjacent spacers. The efficient tuning of their thermal properties can overcome the major challenge of their proper thermal management that limits their stability and prolonged use in devices.

## Conflicts of interest

There are no conflicts to declare.

## Acknowledgements

This work is supported by the Office of Naval Research, Grant No. N00014-21-1-2622. The work is also partially supported by the National Science Foundation (NSF Award No. 2119365). The work at Brown University is partially supported by the Office of Naval Research, Grant No. N00014-20-1-2574.

## References

1 M. Grätzel, *Nature materials*, 2014, **13**, 838–842.
2 Q. Dong, Y. Fang, Y. Shao, P. Mulligan, J. Qiu, L. Cao and J. Huang, *Science*, 2015, **347**, 967–970.
3 H. Zhu, Y. Fu, F. Meng, X. Wu, Z. Gong, Q. Ding, M. V. Gustafsson, M. T. Trinh, S. Jin and X. Zhu, *Nature materials*, 2015, **14**, 636–642.
4 Y. Fang, Q. Dong, Y. Shao, Y. Yuan and J. Huang, *Nature Photonics*, 2015, **9**, 679–686.

5 M. Yuan, L. N. Quan, R. Comin, G. Walters, R. Sabatini, O. Voznyy, S. Hoogland, Y. Zhao, E. M. Beauregard, P. Kanjanaboos *et al.*, *Nature nanotechnology*, 2016, **11**, 872–877.

6 K. Leng, I. Abdelwahab, I. Verzhbitskiy, M. Telychko, L. Chu, W. Fu, X. Chi, N. Guo, Z. Chen, Z. Chen *et al.*, *Nature materials*, 2018, **17**, 908–914.

7 M. H. Du, *Journal of Materials Chemistry A*, 2014, **2**, 9091–9098.

8 S. A. Veldhuis, P. P. Boix, N. Yantara, M. Li, T. C. Sum, N. Mathews and S. G. Mhaisalkar, *Advanced materials*, 2016, **28**, 6804–6834.

9 L. M. Herz *et al.*, *Annu. Rev. Phys. Chem*, 2016, **67**, 65–89.

10 R. L. Milot, R. J. Sutton, G. E. Eperon, A. A. Haghighirad, J. Martinez Hardigree, L. Miranda, H. J. Snaith, M. B. Johnston and L. M. Herz, *Nano letters*, 2016, **16**, 7001–7007.

11 W. A. Dunlap-Shohl, Y. Zhou, N. P. Padture and D. B. Mitzi, *Chemical reviews*, 2018, **119**, 3193–3295.

12 J. Burschka, N. Pellet, S.-J. Moon, R. Humphry-Baker, P. Gao, M. K. Nazeeruddin and M. Grätzel, *Nature*, 2013, **499**, 316–319.

13 S. T. Williams, A. Rajagopal, C.-C. Chueh and A. K.-Y. Jen, *The journal of physical chemistry letters*, 2016, **7**, 811–819.

14 Z. Wei, H. Chen, K. Yan and S. Yang, *Angewandte Chemie International Edition*, 2014, **53**, 13239–13243.

15 Z. Li, T. R. Klein, D. H. Kim, M. Yang, J. J. Berry, M. F. Van Hest and K. Zhu, *Nature Reviews Materials*, 2018, **3**, 1–20.

16 T. M. Brenner, D. A. Egger, L. Kronik, G. Hodes and D. Cahen, *Nature Reviews Materials*, 2016, **1**, 1–16.

17 *National Renewable Energy Laboratory (NREL). Efficiency Chart*, `https://www.nrel.gov/pv/cell-efficiency.html`, Accessed: 2022-7-26.

18 B. Conings, J. Drijkoningen, N. Gauquelin, A. Babayigit, J. D'Haen, L. D'Olieslaeger, A. Ethirajan, J. Verbeeck, J. Manca, E. Mosconi *et al.*, *Advanced Energy Materials*, 2015, **5**, 1500477.

19 I. C. Smith, E. T. Hoke, D. Solis-Ibarra, M. D. McGehee and H. I. Karunadasa, *Angewandte Chemie International Edition*, 2014, **53**, 11232–11235.

20 D. H. Cao, C. C. Stoumpos, O. K. Farha, J. T. Hupp and M. G. Kanatzidis, *Journal of the American Chemical Society*, 2015, **137**, 7843–7850.

21 B. Saparov and D. B. Mitzi, *Chemical reviews*, 2016, **116**, 4558–4596.

22 A. Giri, A. Z. Chen, A. Mattoni, K. Aryana, D. Zhang, X. Hu, S.-H. Lee, J. J. Choi and P. E. Hopkins, *Nano letters*, 2020, **20**, 3331–3337.

23 A. D. Christodoulides, P. Guo, L. Dai, J. M. Hoffman, X. Li, X. Zuo, D. Rosenmann, A. Brumberg, M. G. Kanatzidis, R. D. Schaller *et al.*, *ACS nano*, 2021, **15**, 4165–4172.

24 C. Li, H. Ma, T. Li, J. Dai, M. A. J. Rasel, A. Mattoni, A. Alatas, M. G. Thomas, Z. W. Rouse, A. Shragai, S. P. Baker, B. J. Ramshaw, J. P. Feser, D. B. Mitzi and Z. Tian, *Nano Letters*, 2021, **21**, 3708–3714.

25 M. A. J. Rasel, A. Giri, D. H. Olson, C. Ni, P. E. Hopkins and J. P. Feser, *ACS Applied Materials & Interfaces*, 2020, **12**, 53705–53711.

26 C. Ge, M. Hu, P. Wu, Q. Tan, Z. Chen, Y. Wang, J. Shi and J. Feng, *The Journal of Physical Chemistry C*, 2018, **122**, 15973–15978.

27 G. A. Elbaz, W.-L. Ong, E. A. Doud, P. Kim, D. W. Paley, X. Roy and J. A. Malen, *Nano letters*, 2017, **17**, 5734–5739.

28 C. C. Stoumpos, D. H. Cao, D. J. Clark, J. Young, J. M. Rondinelli, J. I. Jang, J. T. Hupp and M. G. Kanatzidis, *Chemistry of Materials*, 2016, **28**, 2852–2867.

29 C. J. Dahlman, R. A. DeCrescent, N. R. Venkatesan, R. M. Kennard, G. Wu, M. A. Everest, J. A. Schuller and M. L. Chabinyc, *Chemistry of Materials*, 2019, **31**, 5832–5844.

30 Y. Qin, H. Zhong, J. J. Intemann, S. Leng, M. Cui, C. Qin, M. Xiong, F. Liu, A. K.-Y. Jen and K. Yao, *Advanced Energy Materials*, 2020, **10**, 1904050.

31 C. C. Stoumpos, C. M. M. Soe, H. Tsai, W. Nie, J.-C. Blancon, D. H. Cao, F. Liu, B. Traoré, C. Katan, J. Even *et al.*, *Chem*, 2017, **2**, 427–440.

32 A. J. Schmidt, *PhD thesis*, Massachusetts Institute of Technology, 2008.

33 D. G. Cahill, *Review of scientific instruments*, 2004, **75**, 5119–5122.

34 P. E. Hopkins, J. R. Serrano, L. M. Phinney, S. P. Kearney, T. W. Grasser and C. T. Harris, *Journal of Heat Transfer*, 2010, **132**, year.

35 A. J. Schmidt, X. Chen and G. Chen, *Review of Scientific Instruments*, 2008, **79**, 114902.

36 L. Mao, W. Ke, L. Pedesseau, Y. Wu, C. Katan, J. Even, M. R. Wasielewski, C. C. Stoumpos and M. G. Kanatzidis, *Journal of the American Chemical Society*, 2018, **140**, 3775–3783.

37 A. Mattoni, A. Filippetti, M. Saba, C. Caddeo and P. Delugas, *The Journal of Physical Chemistry Letters*, 2016, **7**, 529–535.

38 C. Caddeo, A. Filippetti and A. Mattoni, *Nano Energy*, 2020, **67**, 104162.

39 A. Mattoni and C. Caddeo, *The Journal of Chemical Physics*, 2020, **152**, 104705.

40 P. Delugas, C. Caddeo, A. Filippetti and A. Mattoni, *The journal of physical chemistry letters*, 2016, **7**, 2356–2361.

41 A. Mattoni, A. Filippetti, M. Saba and P. Delugas, *The Journal of Physical Chemistry C*, 2015, **119**, 17421–17428.

42 P. K. Schelling, S. R. Phillpot and P. Keblinski, *Physical Review B*, 2002, **65**, 144306.

43 Y. Moritomo and Y. Tokura, *The Journal of chemical physics*, 1994, **101**, 1763–1766.

44 F. Aguado, F. Rodríguez, R. Valiente, J.-P. Itie and M. Hanfland, *Physical Review B*, 2012, **85**, 100101.

45 A. Jaffe, Y. Lin, W. L. Mao and H. I. Karunadasa, *Journal of the American Chemical Society*, 2015, **137**, 1673–1678.

46 M. D. Smith, L. Pedesseau, M. Kepenekian, I. C. Smith, C. Katan, J. Even and H. I. Karunadasa, *Chemical science*, 2017, **8**, 1960–1968.

47 A. Jaffe, Y. Lin and H. I. Karunadasa, *ACS Energy Letters*, 2017, **2**, 1549–1555.

48 A. Jaffe, Y. Lin, C. M. Beavers, J. Voss, W. L. Mao and H. I. Karunadasa, *ACS central science*, 2016, **2**, 201–209.

49 A. Jaffe, Y. Lin, W. L. Mao and H. I. Karunadasa, *Journal of the American Chemical Society*, 2017, **139**, 4330–4333.

50 L. Mao, C. C. Stoumpos and M. G. Kanatzidis, *Journal of the American Chemical Society*, 2018, **141**, 1171–1190.

51 D. Umeyama, Y. Lin and H. I. Karunadasa, *Chemistry of Materials*, 2016, **28**, 3241–3244.